Catalysis Letters
https://doi.org/10.1007/s10562-022-04178-x

One-Pot Transformation of Citronellal to Menthol Over H-Beta Zeolite Supported Ni Catalyst: Effect of Catalyst Support Acidity and Ni Loading

Somayeh Taghavi[1,2] · Päivi Mäki-Arvela[1] · Zuzana Vajglová[1] · Markus Peurla[3] · Ilari Angervo[4] · Kari Eränen[1] · Elena Ghedini[2] · Federica Menegazzo[2] · Mojgan Zendehdel[5] · Michela Signoretto[2] · Dmitry Yu. Murzin[1]

Received: 10 June 2022 / Accepted: 12 September 2022

Abstract

Citronellal was converted to menthol in a one-pot approach using H-Beta zeolite-based Ni catalyst in a batch reactor at 80 °C, under 20 bar of total pressure. The effects of H-Beta acidity (H-Beta-25 with the molar ratio $SiO_2/Al_2O_3 = 25$ and H-Beta-300 with $SiO_2/Al_2O_3 = 300$) and Ni loading (5, 10 and 15 wt %) on the catalytic performance were investigated. Ni was impregnated on H-Beta support using the evaporation-impregnation method. The physico-chemical properties of the catalysts were characterized by XRD, SEM, TEM, ICP-OES, N_2 physisorption, TPR, and pyridine adsorption–desorption FTIR techniques. Activity and selectivity of catalysts were strongly affected by the Brønsted and Lewis acid sites concentration and strength, Ni loading, its particle size and dispersion. A synergetic effect of appropriate acidity and suitable Ni loading in 15 wt.% Ni/H-Beta-25 catalyst led to the best performance giving 36% yield of menthols and 77% stereoselectivity to (±)-menthol isomer at 93% citronellal conversion. Moreover, the catalyst was successfully regenerated and reused giving similar activity, selectivity and stereoselectivity to the desired (±)-menthol isomer as the fresh one.

Graphical Abstract

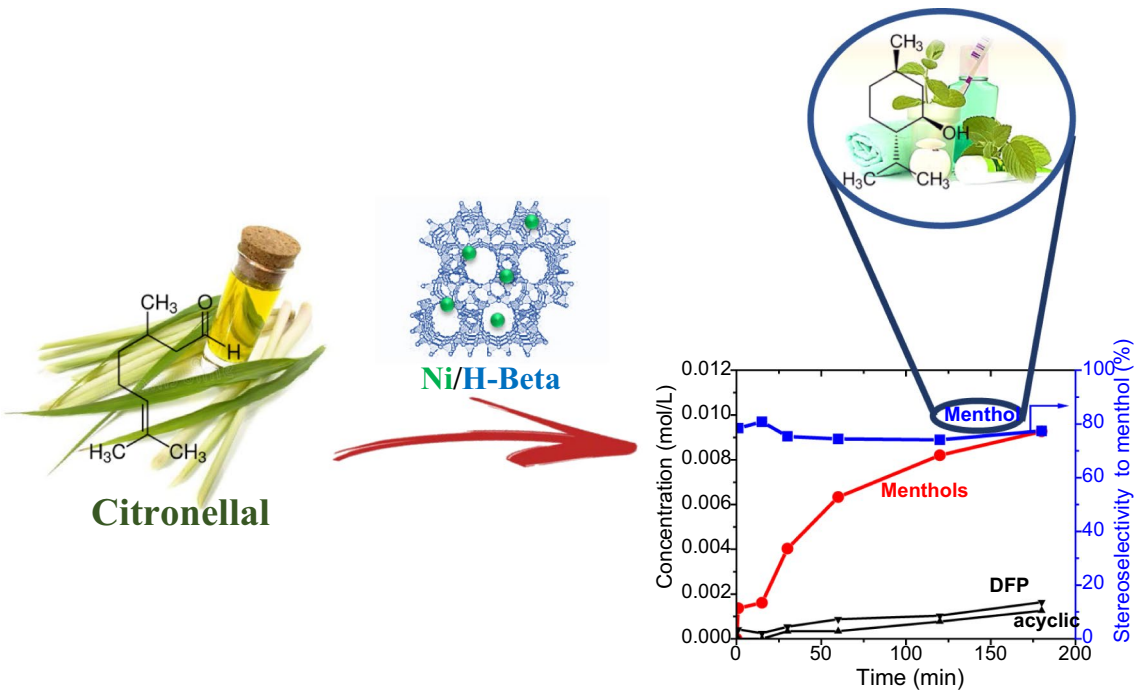

Extended author information available on the last page of the article

Published online: 13 October 2022

Keywords Citronellal · Menthol · H-Beta zeolite · Catalyst acidity · Nickel loading

1 Introduction

Menthol is an organic compound with fresh and cooling sensation being widely used in pharmaceutical, cosmetic and flavoring applications such as ointments, cough drops, toothpaste, mouthwash, chewing gum, candy and perfume [1]. Menthol as a chiral compound can be found with eight possible stereoisomers including: (±)-neomenthol, (±)-menthol, (±)-isomenthol and (±)-neoisomenthol. Among them, (−)-menthol has the most effective cooling sensation [2]. Naturally, menthol was obtained from peppermint essential oil separation, however due to the increasing demand, synthetic menthol was produced by two companies, Haarmann & Reimer and Takasago International Corp. In Haarmann & Reimer process, m-cresol was converted to thymol by propylation followed by hydrogenation to racemic (±)-menthols in the presence of Ru/Al_2O_3 catalyst. Thereafter, (−)-menthol was obtained from racemic (±)-menthols by separation crystallization process [3]. Takasago process was based on conversion of myrcene to (−)-menthol in the presence of Rh- BINAP catalyst [4, 5]. Citral and its derivatives, especially citronellal have attracted significant attention in one-pot menthol synthesis in the recent year [1, 6–16]. Citral can be extracted as an essential oil from distillation of lemongrass oil possessing ca. 70–80% citral inside [11]. In 2004, BASF established a new continuous process for citral production in Ludwigshafen, Germany with annual capacity of 40,000 metric tons [17]. Citral can be selectively hydrogenated to citronellal using metal-supported catalysts. In addition, BASF has also established a technology for production of (+)-(R)-citronellal by direct catalytic hydrogenation of neral or geranial [18]. Hence, in the current work, citronellal was used as a model reactant, and its catalytic transformations to menthol in a batch system were assessed.

Menthol synthesis from citronellal (Scheme 1) proceeds via two steps including citronellal cyclization to pulegols over the acid catalyst followed by their hydrogenation to menthols in the presence of an active metal phase. According to the reaction mechanism, four different enantiomeric pairs of isopulegols and menthols can be produced. In addition, occurrence of side reactions such as hydrogenation of citronellal, dimerization and polymerization, and defunctionalization of citronellal and isopulegol has to be minimized [10].

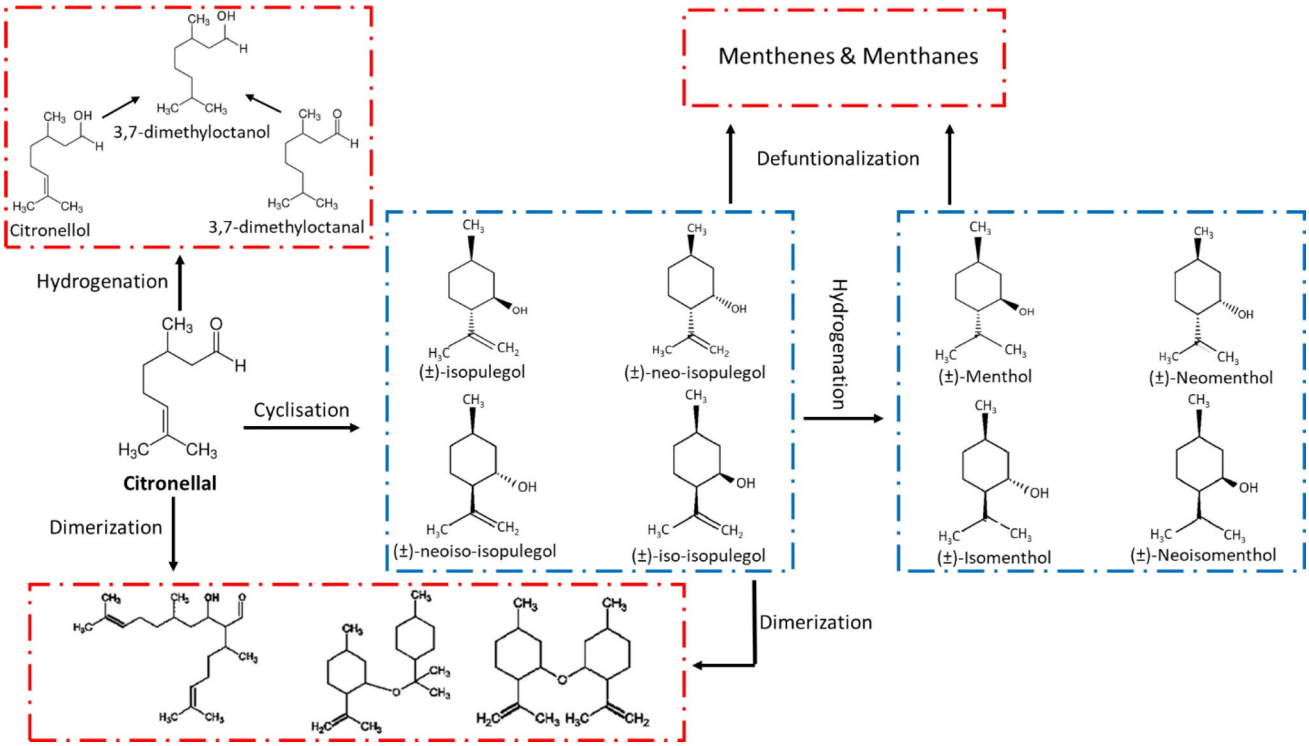

Scheme 1 One-pot synthesis of menthol from citronellal

Hence, selection of an appropriate catalyst to control the reaction pathways toward the desired product is of crucial importance. Due to the apparent drawbacks of homogeneous catalysts such as challenging recovery and separation, along with environmental and economic issues [19], heterogeneous catalysts have attracted much more attention. Various heterogeneous catalysts such as ZrO_2, MCM-41, SiO_2, γ-Al_2O_3 and zeolites were studied for efficient cyclization of citronellal [10, 12, 16, 20–22]. Although majority of the acid catalysts led to high yields of isopulegols, textural and acidic properties of the catalysts were the main factors allowing high stereoselectivity towards (−)-isopulegol. In addition, for the second reaction step, various supported noble and non-noble metals catalysts including Ir, Pd, Pt, Ru, Cu, Ni, Co as an active metal have been used. There are studies in which Beta type zeolites have been used as the catalyst support for the desired reaction [9, 15, 23–25]. Beta zeolite, from BEA topology, is formed by corner-sharing TO4 (T = Si or Al) tetrahedra and is a three-dimensional (3D) crystalline material with three sets of vertical channels and 12-membered ring porous structure. Brønsted acid sites of Beta zeolite are generated after an aqueous ion-exchange using NH_4Cl solutions with subsequent calcination releasing ammonia [26–28].

Plößer et al. performed one-pot transformation of citronellal to menthol using bifunctional metal–acid heterogeneous catalysts, typically Pd, Pt and Ru as the active metals and H-Beta zeolite as the support. Among different catalysts, 1 wt.% Ru/H-Beta-25 was the best one giving the highest menthol selectivity exceeding 93% [15]. In addition, ca. 70% stereoselectivity towards (±)-menthol was obtained using Pt- and Ru- supported H-Beta-25 catalysts both in trickle bed and batch reactors [9]. Noble metals have been used as the catalytically active phases in several other studies exhibiting high activity and selectivity [7, 8, 29, 30]. Moreover, low-cost non-noble metals especially Ni were reported to transform both citral and citronellal to menthol with a high selectivity [23, 24, 31]. For instance, either a bifunctional Ni/Zr-Beta or a dual catalytic system of Zr-Beta and Ni/MCM-41 demonstrated 86–97% yield of menthol with 90–94% diastereoselectivity to (±)-menthol from citronellal. The maximum yield of isopulegol in the first step of the reaction was obtained under He atmosphere in the presence of the acid sites of Beta zeolite with modified Lewis acidity by exchanged Zr. Thereafter, hydrogen was introduced to the system and hydrogenation of isopulegol to menthol was catalyzed by Ni at 80 °C and 20 bar H_2 [23, 24]. A similar strategy was followed in [14] using Ni/γ–Al_2O_3 as the catalyst. The hydrogenation step was carried out under very mild reaction conditions of 90 °C and 1 bar H_2 giving 86% yield of menthols [21]. In addition, one-pot synthesis of menthol from citronellal was catalyzed by sulfated zirconia supported Ni under 14 bar of H_2 and at 100 °C, with enantioselectivity of 88% towards (−)-menthol analyzed with an α-DEX Supelco chiral column [14]. However, sulfated zirconia pillared montmorillonite supported Ni, Ni/ZSM-5 and Ni/natural zeolite exhibited very low activity toward menthol in [6, 16]. One-pot transformation of citral to menthols over different bifunctional catalysts including Ni and Pd as the active phases and H-BEA, SiO_2–Al_2O_3, and Al-MCM-41 as the supports was studied by Trasarti and co-workers [25]. It was suggested that Ni active metal and the solid acid support with mild acidity (Al-MCM-41) could be more active and selective to racemic (±)-menthol giving more than 90% yield of menthols (71% stereoselectivity to (±)-menthol) at full citral conversion at 70 °C, 20 bar H_2, 1 g catalyst, citral/toluene = 2:150 (ml), 5 h.

From the overview given above it is apparently clear that a delicate balance between acidity of a zeolite bearing a pore size favorable for the desired products and the hydrogenation ability of a non- noble cost efficient Ni is required. In the current study beta zeolites with different acidity and Lewis to Brønsted acid sites ratio have been selected as supports for nickel. Loading of latter was varied to adjust the metal dispersion and explore a potential synergy between H-Beta acidity and Ni loading and dispersion to enhance the yield of the main cyclic product (±)-menthol at the same time minimizing the undesired side reactions, which also require the acid sites. Such types of neat H-Beta zeolite supported Ni have never been reported as the catalyst of one-pot transformation of citronellal to menthols in the presence of molecular hydrogen. Subsequently an in-depth study on the synergetic effect of Ni active phase and H-Beta acid sites nature, strength and concentration on the catalytic behavior has been performed. In particular, H-Beta zeolites with two different SiO_2/Al_2O_3 molar ratios, 25 and 300 and Ni loading of 5, 10 and 15 wt% were investigated allowing to correlate the catalysts properties with their reaction performance.

2 Experimental

2.1 Chemicals

The following chemicals were used in the current work: cyclohexane (Alfa Aesar, ≥ 99.9 wt%), racemic (±)-citronellal (Sigma-Aldrich, ≥ 95.0 wt%), menthol (Aldrich, ≥ 99.0 wt%), geraniol (Lancaster, tech. quality), nerol (Sigma-Aldrich, ≥ 97.0 wt%), iso-menthol (Molekula), neomenthol (Fluka, ≥ 97.0 wt%), citronellol (Fluka, ≥ 99.0 wt%), isopulegol (Fluka, ≥ 99.0 wt%).

2.2 Catalyst Preparation

Two different commercial zeolites namely NH_4-Beta-25 (theoretical $SiO_2/Al_2O_3 = 25$ molar ratio) (CP814E) and

H-Beta-300 (theoretical $SiO_2/Al_2O_3 = 300$ molar ratio) (CP811C) were provided from Zeolyst International. Ammonium form NH_4-Beta-25 was transferred to H-beta-25 by stepwise calcination at the final temperature of 400 °C for 4 h. Ni modified H-Beta zeolite supports were prepared by the evaporation impregnation method using nickel (II) nitrate hexahydrate ($Ni(NO_3)_2.6H_2O$, Merck, 99.999%) as the Ni precursor. Different catalysts with nominal Ni-metal loadings of 5, 10 and 15 wt % on H-Beta-25 and H-Beta-300 were synthesized. First, the Ni precursor was dissolved in 250 mL distilled water in a flask and the desired amount of H-Beta support with the sieved fraction below 63 µm to avoid internal mass transfer limitations was added to the solution. The impregnation was carried out in a rotary evaporator with a rotational speed of 10 rpm at room temperature for 24 h. Thereafter, the aqueous solution was evaporated in the rotavapor using a water jet vacuum pump at 50 °C. The obtained catalyst powder was dried at 100 °C for 12 h and calcined in static air at 400 °C for 3 h. The final catalysts were once more sieved below 63 µm. The catalysts were labeled 5Ni/H-Beta-25 (5 wt.% Ni/H-Beta-25), 10Ni/H-Beta-25 (10 wt.% Ni/H-Beta-25), 15Ni/H-Beta-25 (15 wt.% Ni/H-Beta-25), 15Ni/H-Beta-300 (15 wt.% Ni/H-Beta-300).

2.3 Catalyst Characterization

The effective amount of Ni was analyzed by inductively couple plasma–optical emission spectrometry (ICP-OES, PerkinElmer Optima 5300 DV instrument). About 0.1 g of the catalyst was microwave digested with a mixture containing 9 mL of 37% HCl, 3 mL of 65% HNO_3 and 1 mL of 50% HBF_4. After digestion, dilution to 100 mL was done using distilled water.

The X-ray diffraction (XRD) characterization was performed using PANalytical Empyrean diffractometer with five axis goniometers. The incident beam optics consisted of Bragg–Brentano HD X-ray mirror, fixed ¼° divergence slit, 10 mm mask, 0.04 rad soller slit and 1° anti scatter slit. The diffracted beam optics consisted of 7.5 mm divergence slit, 0.04 rad soller slit and PIXcel detector array. The used X-ray tube was Empyrean Cu LFF. The X-ray radiation was filtered to include only Cu Kα1 and Cu Kα2 components. The results were analyzed with MAUD (Material Analysis Using Diffraction) analysis program [32]. Instrumental broadening was evaluated with Si standard sample. The results were obtained with $\theta - 2\theta$ scan range from 5 to 120°.

Scanning Electron Microscopy (Zeiss Leo Gemini 1530) was used to investigate the surface morphology and the shape of the fresh and spent catalysts. 10–15 mg of the catalyst was used for analysis on a thin film coated with activated carbon. SEM images were obtained by using an accelerating voltage of 2.7 kV with a working distance of 2–7 mm.

Transmission Electron Microscopy (TEM, Jeol JEM-14000 plus) was carried out to determine the Ni metal particle size distribution. ImageJ software was used to determine the particle size of Ni from TEM images.

Textural properties were studied by nitrogen physisorption (Micrometrics 3Flex-3500) at − 196 °C. The specific surface area and porosity (pore volume, pore size distribution) were calculated using the Dubinin-Radushkevich (DR) and the density functional theory methods (DFT), respectively, while for the average micropore width and the mesopore diameter the Horvath-Kawazoe and Barrett –Joyner-Halenda methods were used.

Temperature Programed Reduction (TPR) was carried out with a lab-made instrument under 5 vol% H_2 in Ar flow, which was heated from 25 to 800 °C with a ramp of 10 °C/min. The effluent gases were analyzed by a Micrometrics TPDTPR 2900 analyzer equipped with a TCD detector (Gow-Mac 24-550 TCD instrument CO, Bethlehem, PA, USA).

Characterization of the Brønsted and Lewis acid sites, their amount and strength were performed using pyridine (Sigma Aldrich, ≥ 99.5%) adsorption–desorption with FTIR method. The measurements were performed with ATI Mattson FTIR using ca. 20 mg of the catalyst pellet. The catalyst was pretreated in the IR cell by heating from room temperature to 450 °C under vacuum (1×10^{-4} Pa). In order to discriminate between weak, medium and strong acid sites, desorption of pyridine was performed at 250 °C, 350 °C and 450 °C, respectively. Pyridine was desorbed for 60 min at each temperature and the spectra were taken at 100 °C. Quantification of Brønsted and Lewis acid sites was done by considering intensity of IR signals at 1545 cm^{-1} and 1455 cm^{-1}, respectively, using the molar extinction factor given by Emeis [33].

2.4 Catalytic Tests

First, the desired weight of calcined catalyst was charged in an ex-situ glass tube to be reduced under H_2 flow of 50 mL/min with the temperature program of 25 °C—ramping 2 °C/min to 400 °C and holding at this temperature for 3 h. After reduction, the system was cooled down to the ambient temperature. To avoid the reduced catalyst oxidation, it was sealed in the reduction tube by adding 10 mL of the reaction solvent, which was cyclohexane in this work.

Citronellal transformations to menthols were performed by loading 400 mg of citronellal, 300 mg of the pre-reduced catalyst with the particle size below < 63 µm and 90 mL of cyclohexane as the solvent into an autoclave. Before the reaction, the reactor was flushed with a mixture of nitrogen (≅95%) and argon (≅5% Ar) supplied by AGA for 10 min. Thereafter, the reactor temperature was increased to the desired level (50,

60 and 80 °C) under H_2 pressure of 20 bar (99.99%, AGA). The reaction, which duration was 3 h, commenced after reaching the desired temperature by initiating stirring with the rate of 900 rpm. The small catalyst particle size and high stirring speed were used to suppress external and internal mass transfer limitations. The liquid samples of the reaction mixture were taken at certain intervals, diluted with cyclohexane and analyzed by an Agilent GC 6890 N. The GC was equipped with an FID detector at 340 °C and DB-1 column (length 30 m, internal diameter 250 µm and film thickness 0.5 µm). The following temperature program was used for GC-analysis: 110 °C—0.4 °C/min—130 °C—13 °C/min—200 °C (held 5 min). The types of products were confirmed with an Agilent GC/MS 6890 N/5973 N using a DB-1 column (length 30 m, internal diameter 250 µm and film thickness 0.5 µm). For catalyst regeneration, the final solution of the reaction after 3 h was filtered and the solid catalyst on the filter was collected and washed several times with cyclohexane. Thereafter, the spent catalyst was dried at 100 °C for 12 h, reduced with a similar procedure as for the fresh one with the aim to reduce NiO formed during the catalyst recovery, and subsequently used in the second reaction run.

The citronellal conversion, the yield and selectivity, the reaction rate and turnover frequency were calculated using the following equations:

$$X\,(\%) = \frac{C_0 - C_i}{C_0} \times 100 \tag{1}$$

where X is the conversion of citronellal at time t, C_0 and C_i correspond to the molar concentration (mol L^{-1}) of citronellal at time zero and t, respectively,

$$S_p(\%) = \frac{C_p}{\sum \left(C_a + C_b + C_c + \ldots + C_z\right)} \times 100 \tag{2}$$

$$Y_p\,(\%) = \frac{C_p}{C_o} \times 100 \tag{3}$$

where S_p and Y_p are the selectivity and yield of the product p at a certain conversion, respectively, C_p and $(C_a + C_b + C_c + \cdots + C_z)$ correspond to the molar concentrations (mol L^{-1}) of the product p and all products at the same conversion, respectively,

$$r_0 = \frac{\Delta n}{\Delta t.m_{cat}} \text{mol s}^{-1}\text{g}^{-1} \tag{4}$$

$$\text{Initial TOF} = \frac{\Delta n}{\Delta t.n_{metals}} \text{s}^{-1} \tag{5}$$

where r_0 is the initial reaction rate and initial TOF is the initial turnover frequency, $\Delta n/\Delta t$ corresponds to the number of reacted moles per time interval between 1 and15 min, m_{cat} is the mass of catalyst, n_{metals} is the moles of exposed Ni active metal ((moles of Ni in the catalyst) × (dispersion/100)).

3 Results and Discussion

3.1 Catalyst Characterization

The ICP results show that the Ni loading of all catalysts was very close to the nominal value (Table 1). The N_2

Table 1 Ni loading (determined by ICP-OES) and textural properties (obtained from N_2 physisorption) for studied catalysts

Catalysts	Ni loading [wt%]	A_{DR}[a] [m^2/g]	V_{micro} [cm^3/g][b]	V_{meso} [cm^3/g] [b]	Average micropore width,[nm][c]	Average mesopore diameter, [nm][d]	SiO_2/Al_2O_3 [mol/mol][e]
H-Beta-300	–	634	0.25	0.05	0.69	4.9	102
H-Beta-25	–	750	0.26	0.70	0.73	10.0	25
15Ni/H-Beta-300	14.3	406	0.17	0.03	0.66	5.3	–
15Ni/H-Beta-300-spent	–	335	0.14	0.04	0.66	6.4	–
15Ni/H-Beta-25	13.8	383	0.15	0.18	0.66	16.7	–
15Ni/H-Beta-25-spent	–	324	0.12	0.28	0.69	18.5	–
15Ni/H-Beta-25-spent2	–	266	0.10	0.25	0.69	20.0	–
10Ni/H-Beta-25	9.9	516	0.20	0.38	0.67	17.2	–
10Ni/H-Beta-25-spent	–	422	0.16	0.37	0.68	19.0	–
5Ni/H-Beta-25	4.6	524	0.20	0.38	0.67	17.2	–
5Ni/H-Beta-25-spent	–	339	0.13	0.33	0.70	19.2	–

[a]Specific surface area calculated by Dubinin-Radushkevich method (DR)

[b]Calculated by DFT

[c]Calculated by the Horvath-Kawazoe method

[d]Calculated by the BJH method

[e]Calculated by EDX technique[38]

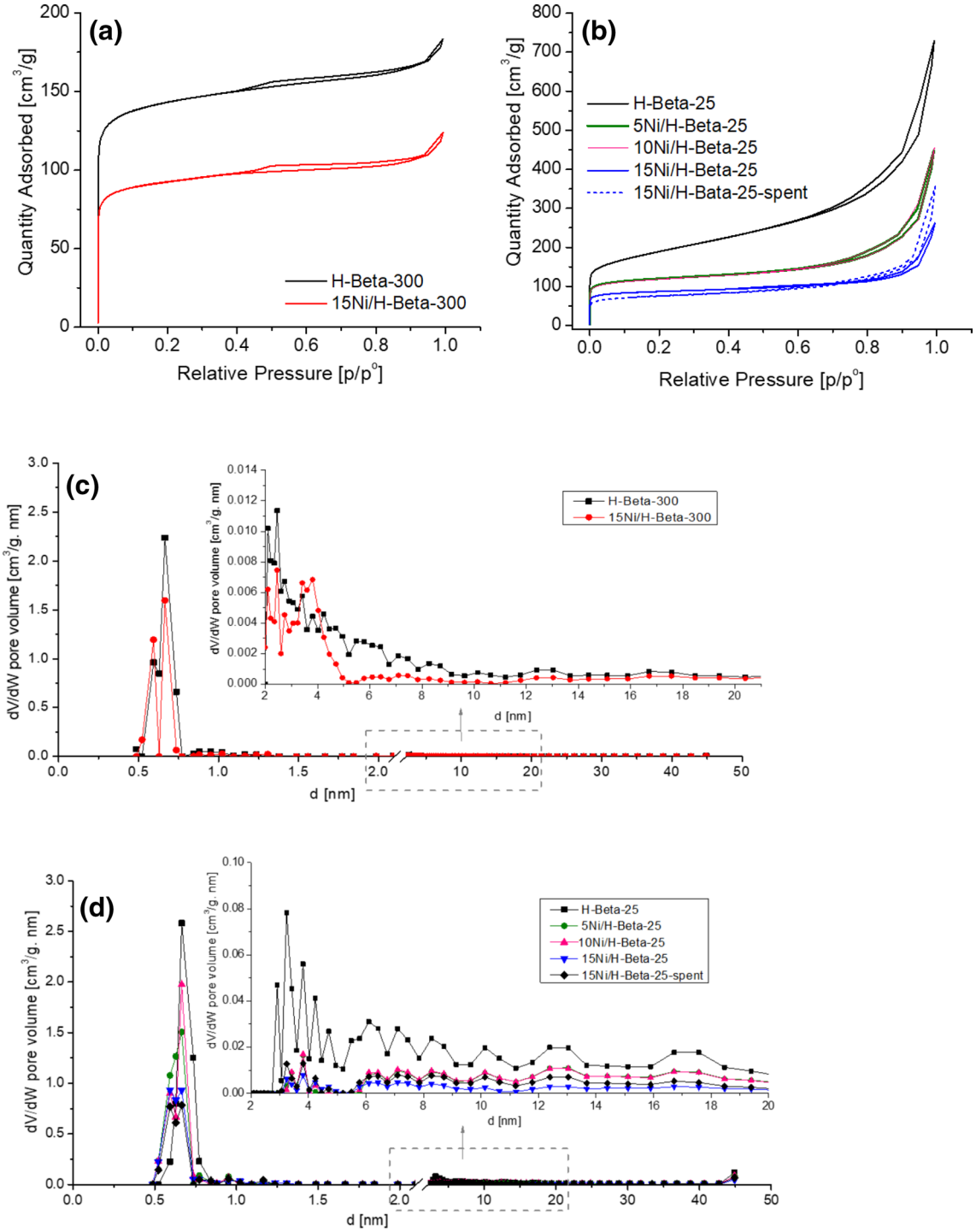

Fig. 1 N_2 adsorption–desorption isotherms and pore size distribution of **a**,**c** H-Beta-300 and 15Ni/H-Beta-300; and **b**,**d** H-Beta-25, 5Ni/H-Beta-25, 10Ni/H-Beta-25, 15Ni/H-Beta-25 and 15Ni/H-Beta-25-spent, respectively

adsorption–desorption isotherms of the parent H-Beta-300 and H-Beta-25 zeolites and the respective catalysts loaded with Ni are shown in Fig. 1. A combination of I and IV type isotherms can be seen for all samples reflecting the coexistence of micropores (ca.80 vol% for Beta-300 catalysts and ca. 30 vol% for Beta-25 catalysts) and mesopores in all materials similar with the results reported in the literature [34]. In particular, a sharp increase of the uptake displayed at a low P/P^0 pressure is assigned to the microporous structure of materials, whereas the hysteresis loops at

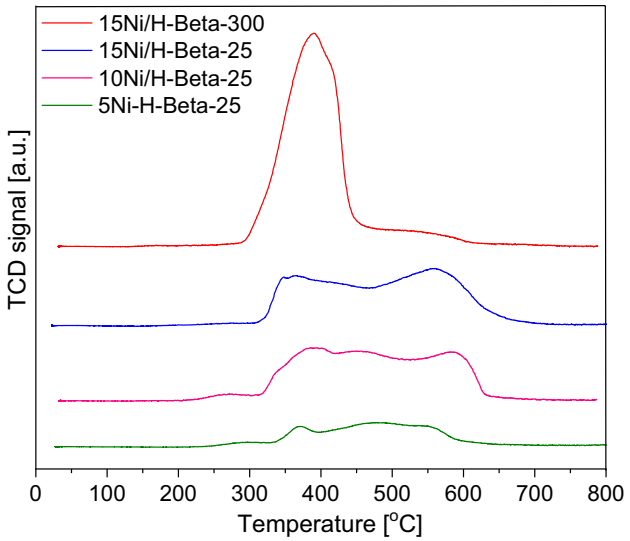

Fig. 2 Hydrogen TPR profiles of the catalysts

Table 2 Results from hydrogen TPR

Catalyst	Normalized peak area in H_2 TPR	T_{max1} [°C]	T_{max2} [°C]
15Ni/H-Beta-300	3.5	390	550
15Ni/H-Beta-25	2.5	365	558
10Ni/H-Beta-25	2.5	393	450, 582
5Ni/H-Beta-25	1	370	480, 545

about $0.5 < P/P^0 < 0.9$ and $0.6 < P/P^0 < 0.9$ are related to the inter-crystalline mesopores of H-Beta-300 and H-Beta-25, respectively [35]. After impregnation of Ni on both zeolites, the shape of isotherms of catalysts stayed unchanged suggesting that the crystalline structure and the zeolites textures were maintained. According to the data in Table 1 and pore size distribution of Fig. 1c,d, by impregnation of Ni on both H-Beta-300 and H-Beta-25 zeolites, a decrease of surface area and pore volume occurred as could be anticipated after Ni introduction into zeolites [36]. Moreover, a further decrease of H-Beta-25 surface area by increasing Ni loading was related to a partial blockage of primary micro-mesopores [37]. Analysis of the textural properties of the 15Ni/H-Beta-25 catalyst after the first and second catalytic run (Fig. 1, Table 1), 5Ni/H-Beta-25, 10Ni/H-Beta-25 and 15Ni/H-Beta-300 after first catalytic run (Table 1) allowed to conclude that the fresh and spent 15Ni/H-Beta-25 catalysts exhibited similar isotherms, and subsequently the catalyst texture was maintained during the reaction. However, surface areas and the micropores volume of all spent catalysts decreased, while mesopores volume increased compared to the fresh ones. This could be described by the blockage of some pores of the catalysts with agglomerated Ni particles, polymeric solid byproducts and also by coke formation [9].

TPR profiles show a complete reduction of NiO in all catalysts at the temperature below 650 °C (Fig. 2). The shape, area and temperature of the peaks in TPR profiles of different catalysts were related to Ni loading, particles size, dispersion and metal interaction with H-Beta support (Fig. 2, Table 2).

In all catalysts, the first peak at the temperature lower than 400 °C is related to the reduction of NiO to Ni^0 mostly located on the surface of H-Beta support with weaker interactions [39]. 5Ni/H-Beta-25 and 10Ni/H-Beta-25 exhibited a second reduction peak at 480 °C and 450 °C, respectively, while for all catalysts a reduction peak with different intensity was present at the temperature higher than 500 °C. These peaks could be related to the reduction of NiO in the intracrystalline mesopores or isolated Ni^{2+} inside the pores of the H-Beta support [37, 40]. The location of metal particles inside the zeolite pores could be strongly related to their loading, size and dispersion. It was suggested that during catalyst impregnation with a low Ni loading, some Ni^{2+} could be ion-exchanged with the protons of hydroxyl groups in the H-Beta channels wall and Ni is thus stabilized close to the zeolite sites. In addition, a part of the intracrystalline NiO during calcination could react with bridging protons (Si–OH–Al) of H-Beta forming $Ni(OH)^+$ [41, 42]. Since the isolated Ni^{2+} ions, NiO and also $Ni(OH)^+$ located in the zeolite pores exhibited strong interactions with H-Beta structure, their reduction was more difficult and occurred at a higher temperature [43]. For this reason, 5Ni/H-Beta-25 and 10Ni/H-Beta-25 with lower Ni loadings, smaller Ni particle sizes and higher dispersions (Fig. 2 and Table 2) exhibited two reduction peaks appearing at the higher temperatures. In addition, a low Ni loading in 5Ni/H-Beta-25 led to the smallest peak area in H_2-TPR and lowest H_2 consumption (Table 2).

Relatively more intracrystalline NiO particles might exist in 15Ni/H-Beta-25 for which only one reduction peak was visible in TPR profile at a higher temperature (558 °C). It was reported that a higher Ni loading can lead to a progressive segregation of NiO phase from zeolite surface to the bulk [40]. On the other hand, 15Ni/H-Beta-300 with the highest Ni loading exhibited the largest H_2-TPR peak area (Table 2) and a different TPR profile. The intensity of the first reduction peak at 390 °C was very high and the second reduction peak at 550 °C had a very low intensity. It can be suggested that majority of NiO particles had weak interactions with the H-Beta-300 support and also that the ion-exchange was less prominent. H-Beta with a very high SiO_2/Al_2O_3 molar ratio of 102 exhibits a hydrophobic nature and a very low Al content in the structure diminishing NiO interactions with the support [44].

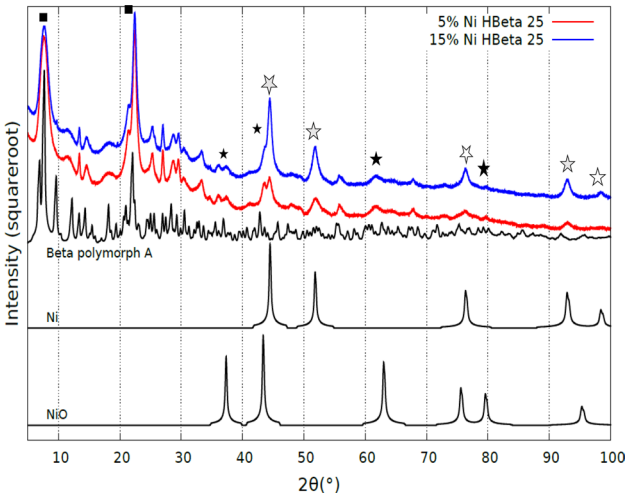

Fig. 3 High-angle XRD patterns of the reduced 5Ni/H-Beta-25 and 15Ni/H-Beta-25 catalysts; (■ H-Beta-25, ☆ Ni.^{0}, ★ NiO)

The XRD patterns of 5Ni/H-Beta-25 and 15Ni/H-Beta-25 catalysts are presented in Fig. 3 illustrating that for both catalysts, there are two main reflexes at 2Θ of 7.8° and 22.3° which are typical for Beta zeolites with a well crystalline structure in line with the literature [45, 46]. The reflexes at 2Θ of 44.4°, 51.8°, 76.4° and 93° are ascribed to metallic Ni^0. The intensities of the lines related to metallic Ni^0 enhanced by increasing the nickel loading. In addition, a small shoulder in the XRD pattern of 15Ni/H-Beta-25 and one of the double-line in XRD pattern of 5Ni/H-Beta-25 located at 2Θ = 43.4° correspond to intracrystalline NiO and demonstrate that the reduction at 400 °C may not completely convert Ni^{2+} to metallic Ni^0 or reoxidation of Ni^0 in the air might happen prior to XRD measurement leading to the presence of a small amount of NiO particles in the catalysts [47–49]. This result agrees well with TPR results (Fig. 2). Thus, it seems that both Ni^0 and NiO (Ni-NiO) were present in the final catalysts being essential for the catalytic reaction. In addition, a comparison between the XRD profile of the support with the catalysts shows that some amorphization occurred in zeolite during the catalyst preparation. It can be

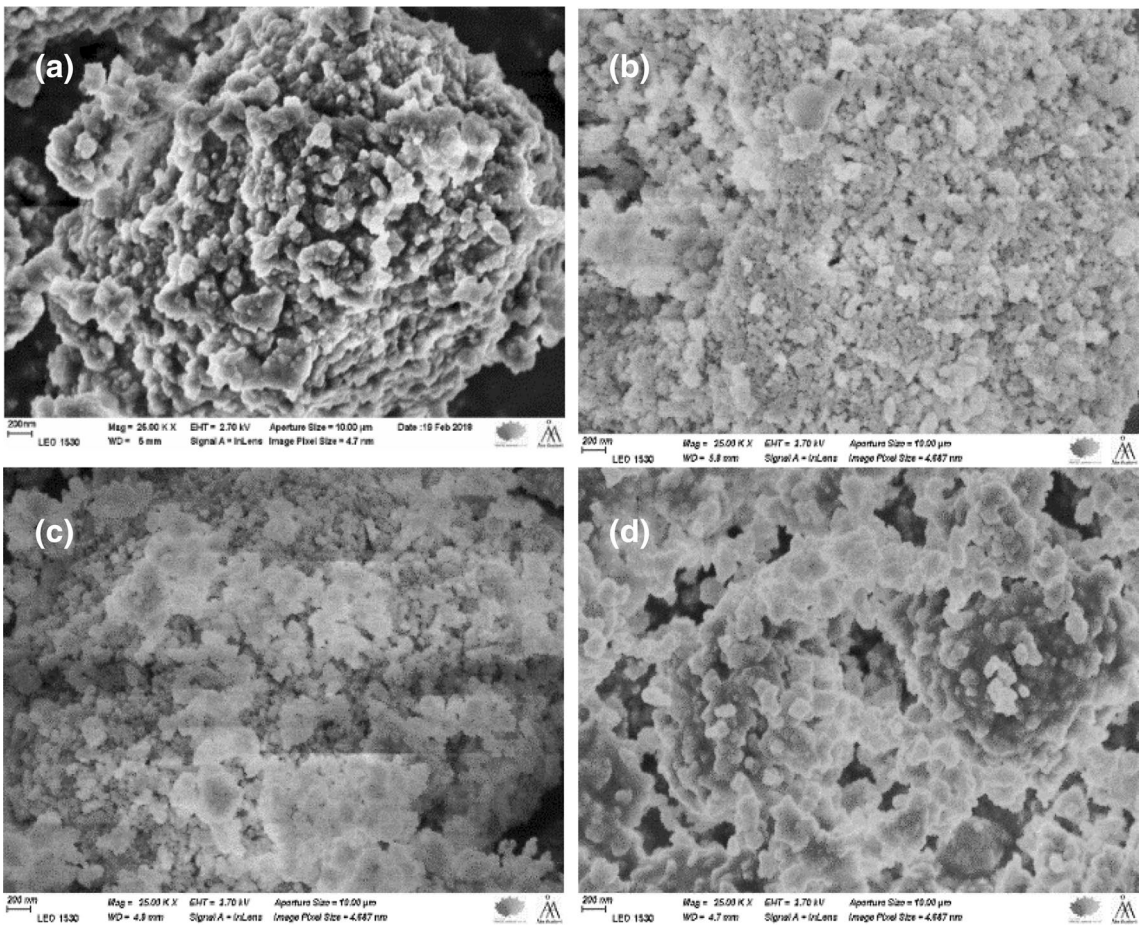

Fig. 4 SEM images of **a** H-Beta-25, **b** 5Ni/H-Beta-25, **c** 15Ni/H-Beta-25 and **d** 15Ni/H-Beta-25-spent. (The magnification of all images is 25.00 K X)

assumed that partial amorphization might happen either at the step of the aqueous solution evaporation under vacuum at 50 °C or most probable at the calcination step. In addition, TPR profiles of the catalysts suggested strong interactions of some NiO and Ni^{2+} ions with the zeolitic structure which might lead to partial amorphization of the zeolite structure at the calcination temperature.

The SEM images of H-Beta-25, 5Ni/H-Beta-25 and 15Ni/H-Beta-25 samples in Fig. 4a–c display that H-Beta-25 has a semi-spherical or round shaped particles typical for Beta-zeolite crystal morphology [50]. However, by incorporation of Ni, especially in 15Ni/H-Beta-25 catalyst with a higher Ni loading, the grain surface of H-Beta zeolite became rough due to the amorphization as was also demonstrated by XRD result. A comparison between the SEM image of the 15Ni/H-Beta-25-spent catalyst with that of the fresh one (Fig. 4c,d) shows that the morphology of Beta-zeolite was almost maintained after the reaction. The SiO_2/Al_2O_3 (mol/mol) ratios of H-Beta-25 and H-Beta-300 were measured by EDX analysis in our previous study [38]. The theoretical SiO_2/Al_2O_3 ratio for H-Beta-25 was close to the experimentally measured ($SiO_2/Al_2O_3 = 25$), while for H-Beta-300 with the theoretical SiO_2/Al_2O_3 ratio of 300, the experimentally measured one was close to 100.

Comparison of the TEM images of the four fresh and reduced catalysts with different Ni loadings and supports (Fig. 5) shows clearly that the particle size distribution for the catalysts with lower metal loadings is narrower due to the presence of smaller Ni-NiO particles, which are less agglomerated. In addition, an increase of the Ni loading led to the enhancement of the average particle size and thus lower dispersion (Table 3). As was confirmed by TPR and XRD results (Fig. 2, Fig. 3), some non-reduced exchanged Ni^{2+}, intercrystallite NiO and $Ni(OH)^+$ could be present besides metallic Ni^0 in the final catalyst. It can be assumed that larger particles in the TEM images of each catalyst could originate from the intercrystallite NiO as was reported by Wang and co-workers [37]. This trend was also visible in other studies reported in the literature [51–53]. In addition, according to TEM for 15Ni/H-Beta-25-spent in Fig. 5c, a slight agglomeration of Ni-NiO nano particles occurred through the reaction increasing the average particle size from 15 nm to 18.4 nm and at the same time particle dispersion decreased from 6.7 to 5.5%. More importantly, the fraction of the Ni-NiO particles bellow 5 nm decreased very much.

The concentration of weak, medium and strong Brønsted and Lewis acid sites of the supports and catalysts was studied by FTIR spectroscopy in the spectrum range of 1400–1575 cm^{-1} using pyridine as the probe molecule. In particular, the weak, medium, and strong acidity was estimated from pyridine desorption for 60 min at each 250 °C, 350 °C and 450 °C, respectively, with quantification of

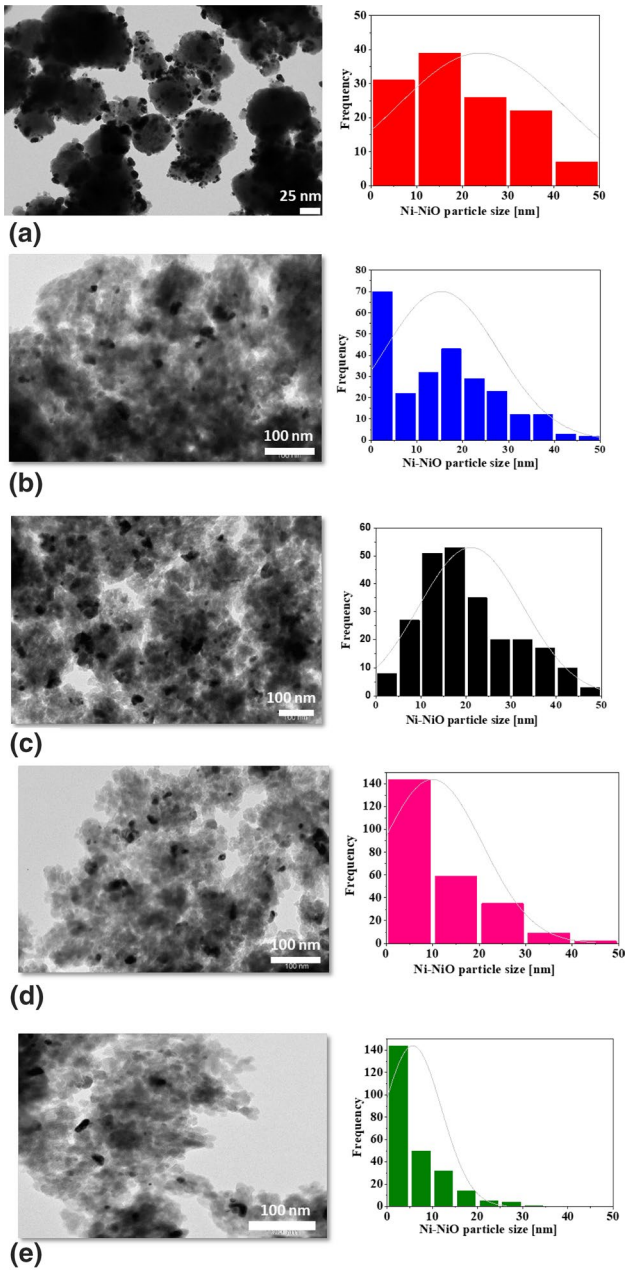

Fig. 5 TEM images and Ni-NiO particle size distribution histograms of reduced **a** 15Ni/H-Beta-300-fresh, **b** 15Ni/H-Beta-25-fresh, **c** 15Ni/H-Beta-25-spent, **d** 10Ni/H-Beta-25-fresh, and **e** 5Ni/H-Beta-25-fresh

Brønsted and Lewis acid sites at each temperature relying on intensity of IR signals at 1545 cm^{-1} and 1455 cm^{-1}, respectively (Fig. 6). As can be seen in pyridine-FTIR results, the Brønsted acid site concentration decreased and the Lewis acid site concentration increased when Ni was loaded on zeolite (Table 4). The decrease of Brønsted acid site concentration could be due to the exchange of protons of the hydroxyl groups in the zeolite channels wall with Ni cations. Moreover, the enhancement of Lewis acid site concentration

Table 3 Average Ni-NiO particle size and dispersion determined from TEM images

Catalyst	Avg. particle size [nm]	Dispersion [%][a]
15Ni/H-Beta-300	19.4	5.2
15Ni/H-Beta-25	15	6.7
15Ni/H-Beta-25-spent	18.4	5.5
10Ni/H-Beta-25	7.5	13.5
5Ni/H-Beta-25	2	50.5

[a]Dispersion [%] = 101/Avg. particle size determined by TEM (nm) [54]

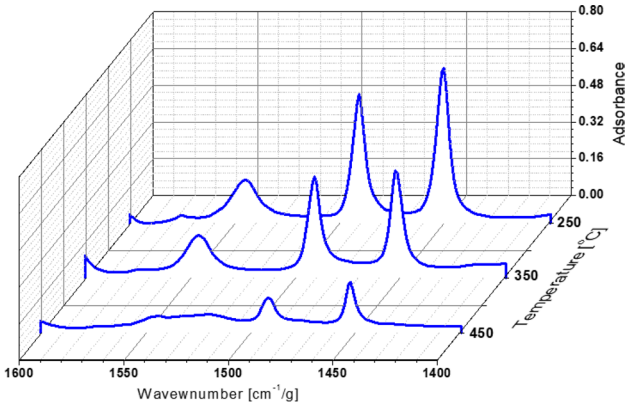

Fig. 6 FT-IR spectra of pyridine adsorption/desorption for 15Ni/H-Beta-25

might be related to incorporation of non-reduced exchanged Ni^{2+} and NiO, and creation of new three-coordinated Al in the zeolite structure during the catalyst preparation step leading to an increase of zeolite amorphous phase as was displayed in XRD patterns (Fig. 3) and SEM images (Fig. 4) of the catalysts. This result agrees well with the previous work of the authors [55]. H-Beta-300 support with the SiO_2/Al_2O_3 molar ratio of 102 (determined by EDX) and 15Ni/H-Beta-300 catalyst exhibited lower concentration of both Lewis and Brønsted acid sites compared to H-Beta-25 with SiO_2/Al_2O_3 molar ratio of 25 and the 15Ni/H-Beta-25 catalyst, respectively. Lewis acidity of the zeolite comes from framework Al located on the edges and also extra-framework Al, while the Brønsted acid sites originate from H^+ ions of hydroxyl groups bridging aluminum and silicon of the channel walls [56]. Therefore, by increasing the SiO_2/Al_2O_3 ratio and hence decreasing both framework and extra-framework Al, both Lewis and Brønsted acidities decrease as could be anticipated and reported numerous times [57, 58]. In addition, by decreasing the Ni loading from 15 to 10% and further to 5% in H-Beta-25 catalysts, a slight increase of Brønsted acid sites concentrations and considerable increase of Lewis acid sites concentrations occurred. This could be related to better accessibility of H-Beta-25 Brønsted and Lewis acid sites when there are less Ni particles blocking the pores and preventing such access. Since catalyst acidity is important for cyclization of citronellal to pulegols [59, 60], it was expected that catalysts with different acidities would display different performances.

3.2 Catalytic Results

The results for one-pot transformation of citronellal in the presence of 15Ni/H-Beta-300, 15Ni/H-Beta-25, 10Ni/H-Beta-25 and 5Ni/H-Beta-25 catalysts are reported in Table 5 and Figs. 7–12. The relative error of GC analysis was generally less than ± 5%.

A comparison of the initial reaction rates and the initial TOFs for different H-Beta-25 supported Ni catalysts presented in Table 5 shows that the most rapid initial reaction and the highest TOF were observed for 5Ni/H-Beta-25 giving a rate of $1.6.10^{-6}$ mol s^{-1} $g_{cat}{}^{-1}$ and TOF of 0.035 s^{-1}. This catalyst exhibited the highest acidity among the studied materials and the smallest Ni-NiO particle size (Tables 3 and 4). On the other hand, a high initial TOF was also obtained over 15Ni/H-Beta-300, which exhibited mild acidity and relatively large Ni-NiO particles, low exposed Ni metal (mole) with a higher Ni loading.

Table 4 Concentration of Brønsted acid sites (B) and Lewis acid sites (L) determined by FTIR with pyridine

Catalysts	250 °C Weak acidity		350 °C Medium acidity		450 °C Strong acidity		Total acid sites [μmol g^{-1}]	B/L
	C_B [μmol g^{-1}]	C_L [μmol g^{-1}]	C_B [μmol g^{-1}]	C_L [μmol g^{-1}]	C_B [μmol g^{-1}]	C_L [μmol g^{-1}]		
H-Beta-300	66	11	50	5	23	3	158	7.3
15Ni/H-Beta-300	12	27	9	8	–	–	56	0.60
H-Beta-25 [61]	53	35	42	17	191	10	349	4.6
15Ni/H-Beta-25	10	59	74	55	5	31	234	0.61
10Ni/H-Beta-25	6	76	91	92	14	35	313	0.55
5Ni/H-Beta-25	8	84	81	98	5	49	325	0.41

Table 5 Catalytic reaction results of one-pot transformation of citronellal to menthol. Conditions: 80 °C, 20 bar H_2, solvent: cyclohexane, amount of catalyst: 300 mg, the initial citronellal concentration: 0.029 M. Conversion of citronellal (X) is given at 3 h of reaction time. Yields (Y) of different products, stereoselectivity (SS), are given at 85% conversion out of round bracket and after 3 h of the reaction in the round bracket

Catalyst	r_0 [mol/s.g_{cat}]	Initial TOF [s^{-1}]	X [%]	Y_{Ps} [%]	Y_{MEs} [%]	Y_{ACP} [%]	Y_{CP}/Y_{ACP}	Y_{DM} [%]	SS_{ME} [%]
15Ni/H-Beta-300	$2.4.10^{-7}$	0.058	88	9.1 (7)	30 (32)	7 (8)	6.6 (5.9)	31.8 (33)	79 (80)
15Ni/H-Beta-25	$6.6.10^{-7}$	0.023	93	19.8 (11)	31.2 (36)	2.6 (4)	21 (13.2)	28 (35)	74 (77)
10Ni/H-Beta-25	$6.7.10^{-7}$	0.024	96	33.2 (13)	21.7 (36)	2.3 (2)	24.7 (27)	25 (39)	78 (77)
5Ni/H-Beta-25	$1.6.10^{-6}$	0.035	98	51.1 (21)	3.6 (26)	1.5 (1)	36.8 (49)	28 (48)	83 (79)

X conversion; *Y* yield; r_0 initial reaction rate; *Ps* pulegols = (±)-isopulegol (IP) + (±)-neoisopulegol (NIP) + (±)-isoisopulegol (IIP) + (±)-neoisopulegol (NIIP); *MEs* menthols: (±)-menthol (ME) + (±)-neomenthol (NME) + (±)-isomenthol (IM) + (±)-neoisomenthol (NIM); *CP* cyclic products: pulegols + menthols + defunctionalization products (DFP); *ACP* acyclic monomeric products: citronellol (CLOL) + 3,7-dimethyloctanol (DMO) + 3,7-dimethyloctane (DME); *DM* dimeric ethers; SS_{ME} stereoselectivity of menthol = ME/ΣMEs

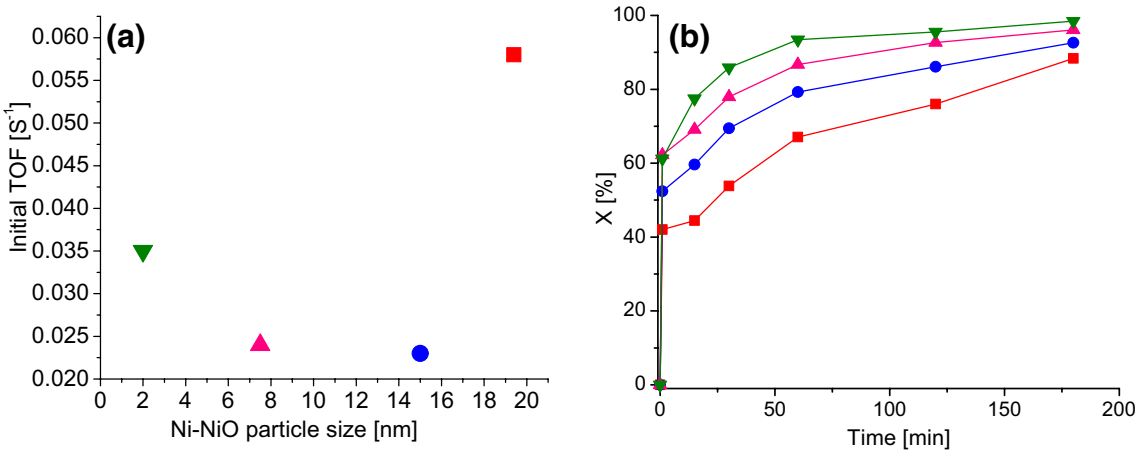

Fig. 7 One pot transformation of citronellal to menthol: **a** The initial TOF as a function of Ni-NiO average particle size and **b** conversion vs time for 15Ni/H-Beta-300 (red ■), 15Ni/H-Beta-25 (blue ●), 10Ni/H-Beta-25 (pink ▲), 5Ni/H-Beta-25 (green▼). Conditions: 80 °C, 20 bar H_2, solvent: cyclohexane, amount of catalyst: 300 mg, the initial citronellal concentration: 0.029 M

The largest peak area in H_2-TPR was observed for 15Ni/H-Beta-300 (Table 2), which, however, exhibited the lowest initial rate. It can be thus stated that the initial transformation rate for citronellal does not only depend on the Ni-NiO particle size, but also on acidity. In particular, citronellal cyclization as well as side reactions, such as etherification, are known to be acid catalyzed [12]. Moreover, as the initial activity of 15Ni/H-Beta-300 is the lowest, the observed behavior is a result of a combined effect of the metal particles and mild acidity. Ni particles were rather large not promoting hydrogenation and under the studied conditions the main reaction in cyclohexane, a hydrophobic solvent, was cyclisation, which occurred slowly due to mild acidity. Both the initial reaction rate and initial TOF decreased by increasing the Ni loading and increasing Ni-NiO particle size (Table 5, Fig. 7a).

Citronellal transformation proceeded in the fastest way over 5Ni/H-Beta-25 with almost 80% of citronellal conversion achieved after 15 min of the reaction. Moreover, this catalyst gave also the highest final conversion of 98% after 3 h, most probably due to the presence of small Ni-NiO particles and high acidity. The conversion increased by decreasing the metal loading (Table 5) and enhancing Lewis acid site concentration (LAS) (Fig. 8a). The same trend was observed in the work of Vajglova et al. by increasing total acid site concentration [1]. All catalysts gave complete mass balance closure of the liquid phase.

The products formation over different catalysts is shown in Table 5 and Fig. 9a,c,e,g. The highest concentration of (±)-isopulegol was already observed after 1 min of reaction, because it was formed during heating in the absence of any stirring. Thereafter, pulegols were reacting further to menthols and menthanes (Fig. 9b, d, f, h). The highest concentration of (±)-isopulegol was obtained after 1 min with 5Ni/H-Beta-25 followed by 10Ni/H-Beta-25, 15Ni/H-Beta-25 and 15Ni/H-Beta-300 which corresponds to the order of decreasing acidity and increasing B/L ratio of H-Beta (Fig. 8d) and increasing Ni loading. This is

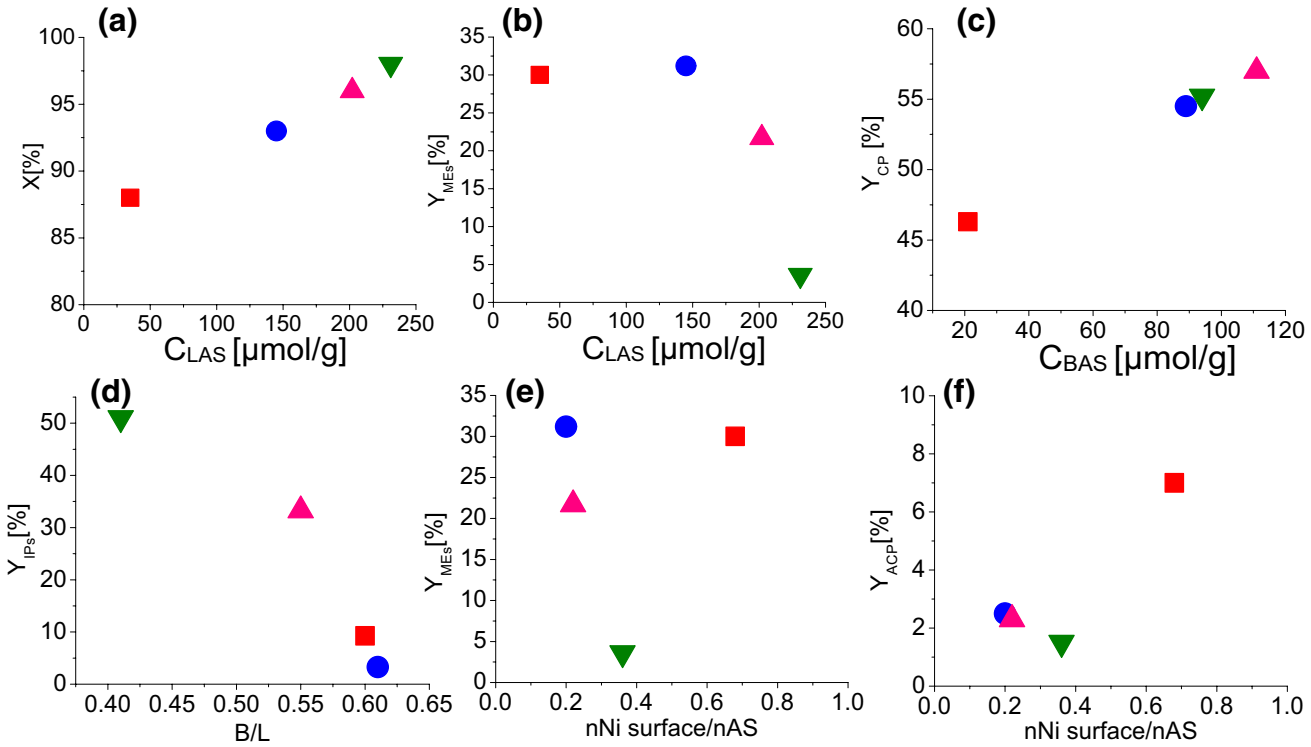

Fig. 8 Menthol synthesis from citronellal **a** citronellal conversion as a function of Lewis acid sites concentration (C_{LAS}); at 85% conversion, **b** yields of menthols (Y_{MEs}) as a function of Lewis acid sites concentration (C_{LAS}); **c** cyclization products yield (Y_{CP}) as a function Brønsted acid sites concentration (C_{BAS}); **d** yield of isopulegols (Y_{IPs}) as a function of Brønsted to Lewis acid sites ratio (B/L) **e** yield of menthols and **f** acyclic products yield as a function of mole of surface metal-to-mole of acid sites ratio. Legend: 15Ni/H-Beta-300 (red ■), 15Ni-H-Beta-25 (blue ●), 10Ni/H-Beta-25 (pink ▲), 5Ni/H-Beta-25 (green▼)

expected, because cyclisation of citronellal is an acid catalyzed reaction [59]. Indeed, Y_{IPs} increased with increasing strong Brønsted acid sites concentration in other studies [1, 62].

In the following step hydrogenation of (±)-isopulegol to (±)-menthol proceeded at a rather low rate over the most acidic 5Ni/H-Beta-25 (Fig. 10) despite of its small Ni-NiO particles. The yield of menthols at 85% conversion level of citronellal decreased with decreasing Ni-NiO particle size and increasing especially Lewis acidity.

This result shows that even rather large Ni-NiO particles of ca. 15 nm facilitated efficient hydrogenation of pulegols to menthols (Fig. 10) and the menthol yield at 85% conversion even increased with increasing Ni-NiO particle size (Fig. 11a).

The maximum yield of menthols, 36% was obtained for 15Ni/H-Beta-25 and 10Ni/H-Beta-25 at 3 h reaction (Table 5). However, neomenthol and neoisomenthol concentrations increased in the first hour of the reaction and reached almost a plateau for all catalysts (Fig. 9). From the concentration profiles for citronellal transformations (Fig. 9), the consecutive nature of the reaction network can be clearly seen and already after 15 min the menthol formation rate increased. Among 5Ni/H-Beta-25, 10Ni/H-Beta-25 and 15Ni/H-Beta-25, the latter exhibited the lowest amount of Brønsted acid sites (Table 4) being superior for menthol formation in comparison to two other catalysts. In the work reported by Murzin and co-workers, Y_{MEs} decreased with increasing Brønsted acid sites concentration [9]. The Brønsted-to-Lewis acid sites ratio (B/L) of this catalyst was 0.6 (Table 4) which is in line with the results for Ni/ZrS (nickel sulfated zirconia) catalyst displaying a higher acid cites concentration of 95 µm/g and a B/L ratio of 0.6 [14]. That catalyst was more active in citronellal transformation to menthols compared to nickel on sulfated zirconia possessing the acid sites concentration of 30 µm/g and a higher B/L ratio of 0.9. The highest menthol yield in [63] was 98% at full citronellal conversion over 8 wt% Ni-montmorillonite-heteropolyacid catalyst at 80 °C, under 50 bar hydrogen and after a longer reaction time of 12 h. This catalyst exhibited the B/L ratio of 0.3, however, the Ni particle size was not reported. It was suggested in [63] that the catalyst with strong Lewis and medium Brønsted acid sites is suitable for the reaction which was also observed in the current study.

Stereoselectivity to (±)-menthol was initially the highest for 5Ni/H-Beta-25, decreasing, however, with increasing

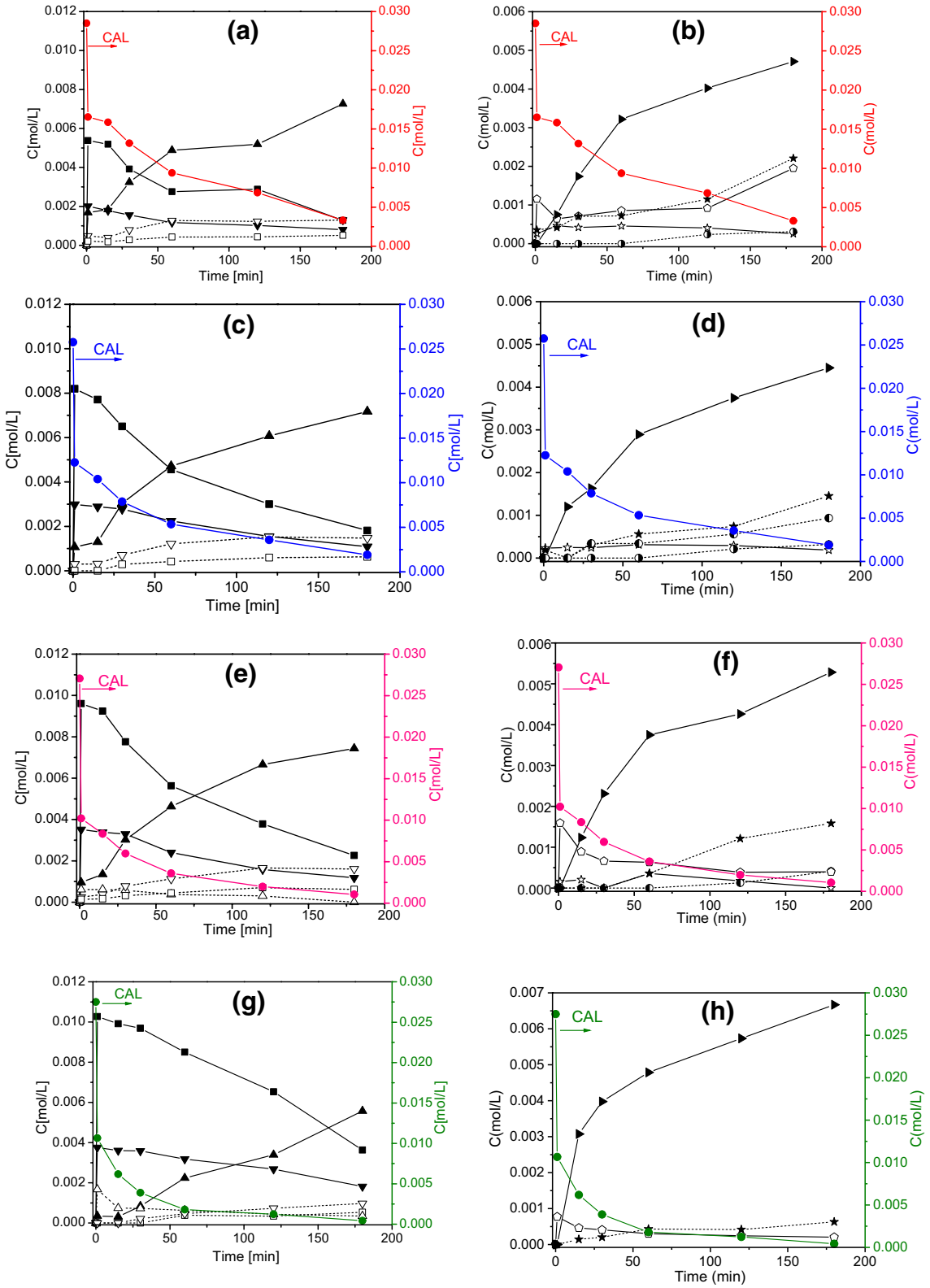

Fig. 9 Menthol synthesis from citronellal for **a**, **b** 15Ni/H-Beta-300, **c**, **d** 15Ni/H-Beta-25, **e**, **f** 10Ni/H-Beta-25 and **g**, **h** 5Ni/H-Beta-25: Concentration of citronellal (●), (±)-isopulegol (■), (±)-neo-isopulegol (▼), (±)-iso-isopulegol (Δ), (±)-menthol (▲), (±)-neomenthol (∇), (±)-neoisomenthol (□), citronellol (⬠), menthanes (☆), 3,7-dimethyloctanol (◑), 3,7-dimethyloctane (◐), dimeric ethers (►). Citronellal concentration presented in all graphs corresponds to right hand side y-axes and color coded: **a**, **b** red; **c**, **d** blue; **e**, **f** pink; **g**, **h**) green. Concentration of all other compounds correspond to the left hand side y-axes

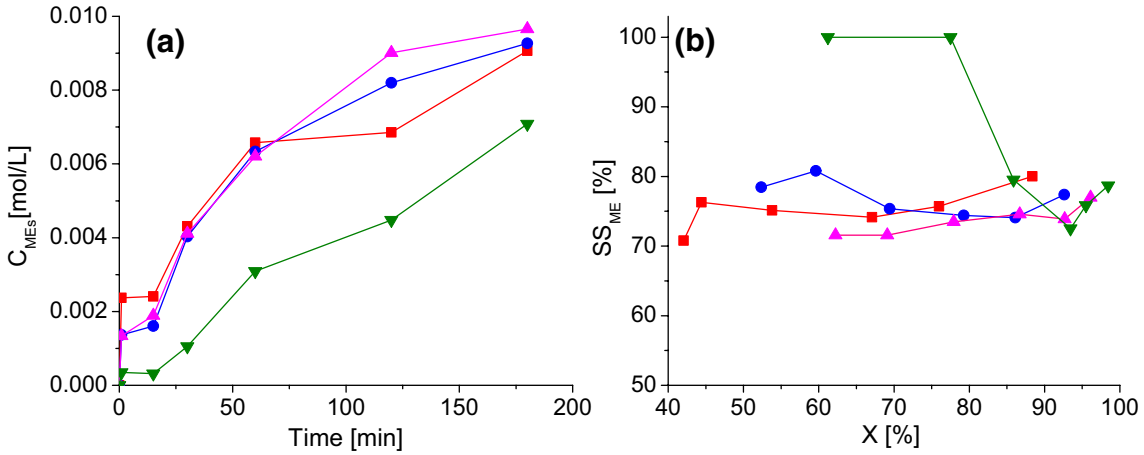

Fig. 10 Menthol synthesis from citronellal: **a** Concentration of menthols as a function of time, **b** stereoselectivity of menthol as a function of conversion. Legend: 15Ni/H-Beta-300 (red ■), 15Ni-H-Beta-25 (blue ●), 10Ni/H-Beta-25 (pink ▲), 5Ni/H-Beta-25 (green▼)

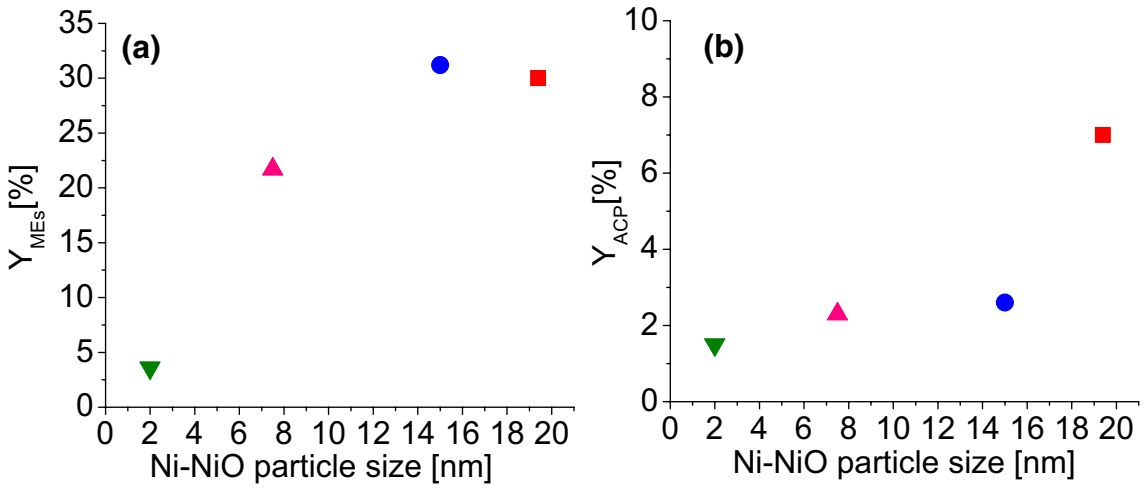

Fig. 11 Menthol synthesis from citronellal, yields of **a** menthols (Y_{MEs}) and **b** ACP (Y_{ACP}) at 85% conversion as a function of Ni@NiO particle size. 15Ni-H-Beta-300 (red ■), 15Ni-H-Beta-25 (blue ●), 10Ni/H-Beta-25 (pink ▲), 5Ni/H-Beta-25 (green▼)

conversion to the same level, ca. 78%, as obtained for other catalysts (Fig. 10b). When comparing the stereoselectivity to (±)-menthol for nickel catalysts reported in the literature [14], it should be mentioned that nickel on sulfated zirconia gave 70% of stereoselectivity to (±)-menthol at a full citronellal conversion, at 100 ℃ and under 14 bar H_2 after 30 min with the citronellal to catalyst mass ratio of 0.6. Note that the reaction in the current work was carried out under conditions different from [14], namely 80 °C, total pressure of 20 bar, reaction time 3 h and the citronellal to catalyst mass ratio of 1.3.

Formation of the undesired acyclic hydrogenation products (ACP), among which the most prominent product was citronellol, increased by increasing the Ni loading and particle size (Fig. 8, Table 3). In addition to citronellol, also small amounts of 3,7-dimethyloctanol were formed. In particular, by increasing the molar ratio of the exposed metal to the acid sites, the yield of ACP decreased for Ni/H-Beta-25 catalysts (Fig. 8f) similar with the result of ref [10], while 15Ni/H-Beta-300 with a mild acidity (Table 4) produced large amounts of both citronellol and 3,7-dimethyloctanol, and no 3,7-dimethyloctanol was formed over 5Ni/H-Beta-25.

Dimer formation was prominent over all studied catalysts (Table 5, Figs. 9). 5Ni/H-Beta-25 as the most acidic catalyst generated the highest concentration of dimeric products (Fig. 9h). Dimer formation was as expected also independent on the Ni-NiO average particle size. As a comparison, a relatively low menthol yield being less than 10% and high byproducts yield of more than 40% were observed at 24–100% citronellal conversion over natural zeolite supported Ni and Ni/ZSM-5 catalysts, respectively [8]. The reaction conditions were very different from the

current work with the citronellal to catalyst mass ratio of 7, 70 °C, 20 bar of H_2 and 7 h reaction time [16]. On the other hand, when the reaction was carried out at a higher temperature of 200 °C and 20 bar H_2, 50% yield of menthol, 10% yield of isopulegol and 35% yield of byproducts were obtained over Ni/NZB (acidified natural zeolite) catalyst [64].

From the viewpoint of the reaction mechanism, it was interesting to relate formation of acyclic hydrogenation products vs cyclic counterparts. For that purpose, the sum of acyclic hydrogenation products (ACP) versus the sum of the desired cyclisation products (CP = IPs + MEs) was plotted (Fig. 12).

For 15Ni/H-Beta-300 with the highest Ni loading and the mild acidity, both the concentration of cyclic and acyclic products increased after 15 min of the reaction time and more acyclic hydrogenation products were formed with increasing reaction time. Due to a mild acidity, cyclisation was not as efficient as with the other catalysts. On the other hand, for 15Ni/H-Beta-25, only cyclic products were produced in the first 15 min of the reaction, thereafter formation of acyclic hydrogenation products started due to suppression of cyclization. 10Ni/H-Beta-25 and 5Ni/H-Beta-25 generated the maximum concentrations of cyclic products after 120 min and 60 min of the reaction, respectively. The highest amounts of acyclic hydrogenation products were formed over 15Ni/H-Beta-300, which exhibited the highest peak area in H_2-TPR (Table 2) and mild acidity (Table 4). On the other hand, the second highest concentration of ACP was obtained over the catalyst with medium acidity and 15 nm Ni-NiO particles (Table 3), while the smallest Ni-NiO particles, 2 nm, present in 5Ni/H-Beta-25 with the highest acidity among the studied Ni/H-Beta catalysts (Table 4) promoted formation of cyclisation products. These results differ slightly from the ones published by Azkaar et al. [9], who reported that highly acidic Ru catalyst promoted ACP formation.

3.3 Regeneration and Reuse of 15 Wt% Ni/H-Beta-25

The characterization results demonstrated stability of the textural and morphological properties of 15Ni-H-Beta-25 catalyst after the reaction. Nevertheless, because minor leaching of Ni could be concluded from ICP-OES measurements, the spent catalyst was regenerated by washing with the reaction solvent (cyclohexane) followed by drying and reduction steps. Thereafter, the regenerated catalyst was tested in the reaction with the results reported in Fig. 13.

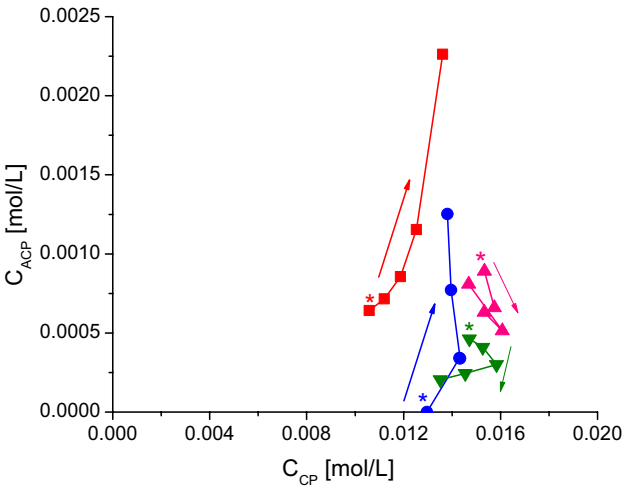

Fig. 12 Sum of hydrogenation acyclic products concentrations (ACP) vs the sum of desired cyclization products concentrations (CP = IPs + MEs) at 80 °C, 20 bar total pressure in the presence of hydrogen for 15Ni/H-Beta-300 (red ■), 15Ni-H-Beta-25 (blue ●), 10Ni/H-Beta-25 (pink ▲), 5Ni/H-Beta-25 (green ▼), first point (*, denoted reaction time 15 min)

It can be concluded that very similar conversion, yields of pulegols and menthols, along with stereoselectivity to (±)-isopulegol and (±)-menthol were obtained in the second run, which is a promising result in terms of catalyst recyclability.

4 Conclusion

Ni/H-Beta catalysts with different silica to alumina ratios and thus acidities (H-Beta-25 and H-Beta-300) and different Ni loadings of 5, 10 and 15 wt.% were prepared and tested in the one-pot transformations of citronellal to menthol in a batch reactor. Different Ni loadings affected the Ni-NiO particle size and dispersion and also accessibility of the H-Beta-25 acid sites. An optimum synergy between H-Beta acidity and Ni loading and dispersion was required to drive the cascade reaction toward the main cyclic product namely (±)-menthol isomer limiting undesired side reactions, such as acyclic hydrogenation and dimerization of citronellal and pulegols. Among the tested materials, 15 wt.% Ni on H-Beta-25 exhibited the best synergy of the total acid sites concentration, Lewis to Brønsted acid sites ratio, and the metal loading and dispersion. The reaction over 15 wt% Ni/H-Beta-25 led to 93% citronellal conversion with the highest menthols yield of 36% (77% stereoselectivity to (±)-menthol isomer). Regeneration and reusability of

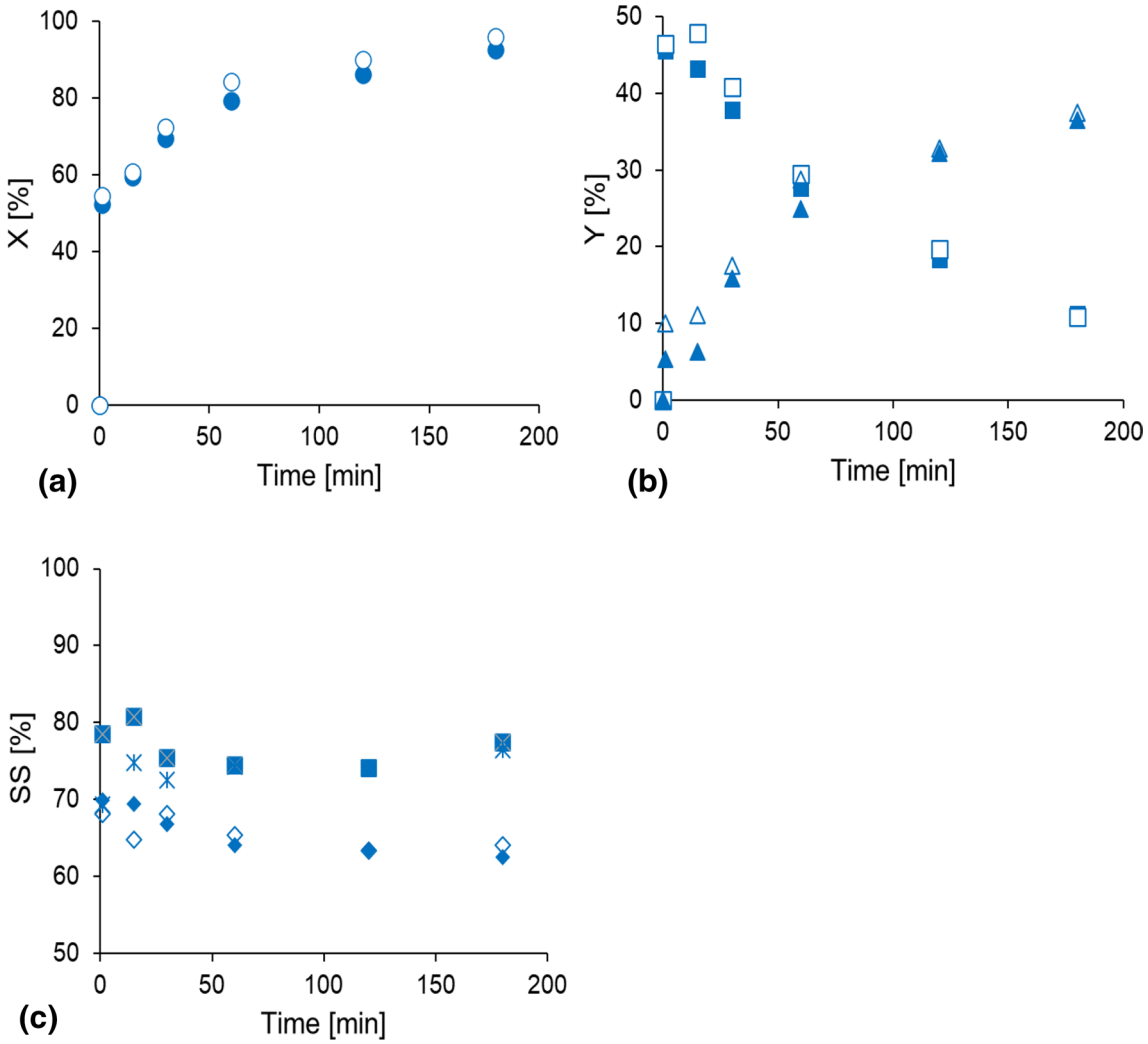

Fig. 13 **a** Conversion of citronellal, X (●, ○), **b** yield of pulegols, Y_{Ps} (■, □) and yield of menthols, Y_{MEs} (▲, Δ), **c** stereoselectivity to (±)-isopulegol (◆, ◊) and (±)-menthol (★, ✱) as a function of time in one-pot synthesis of menthol starting from citronellal over 15Ni/H-Beta-25. Symbols: fresh catalyst (filled symbol), regenerated catalyst (open symbol)

the best catalyst was promising as the reused catalyst after simple washing with the solvent and reduction afforded similar activity and selectivity as the fresh catalyst. While the amount of acyclic products was rather low, dimeric ethers of cyclic nature were formed on acid sites with appreciable selectivity, thus further efforts in modulation of acid/metal bifunctionality should be focused on further improving the yields of the desired menthols in the one-pot conversion of citronellal.

Acknowledgements The authors are grateful to Academy of Finland for funding through the project: Synthesis of spatially controlled catalysts with superior performance. Electron microscopy samples were processed and analyzed at the Electron Microscopy Laboratory, Institute of Biomedicine, University of Turku, which receives financial support from Biocenter Finland. The MIUR (Italian ministry for education, university and research) is gratefully acknowledged for the financial support (doctoral scholarships) of the inter-university Ph.D. program of Trieste University and Ca' Foscari University.

Funding Open access funding provided by Abo Akademi University.

Declarations

Competing Interest The authors declare that they have no known competing financial interests or personal relationships that could have appeared to influence the work reported in this paper.

References

1. Vajglová Z, Kumar N, Mäki-Arvela P et al (2019) Effect of binders on the physicochemical and catalytic properties of extrudate-shaped beta zeolite catalysts for cyclization of citronellal. Org Process Res Dev 23:2456–2463. https://doi.org/10.1021/acs.oprd.9b00346
2. Neaţu F, Coman S, Pârvulescu VI et al (2009) Heterogeneous catalytic transformation of citronellal to menthol in a single step on Ir-beta zeolite catalysts. Top Catal 52:1292–1300. https://doi.org/10.1007/s11244-009-9270-9
3. Davis JC (1978) L-menthol synthesis employs cheap, available feedstocks. Chem Eng (NY) 85:62–63
4. Emura M, Matsuda H (2014) A green and sustainable approach: Celebrating the 30th anniversary of the asymmetric l-menthol process. Chem Biodivers 11:1688–1699. https://doi.org/10.1002/cbdv.201400063
5. Misono M, Nojiri N (1990) Recent progress in catalytic technology in Japan. Appl Catal 64:1–30. https://doi.org/10.1016/S0166-9834(00)81550-X
6. Fatimah I, Rubiyanto D, Huda T et al (2015) Ni dispersed on sulfated zirconia pillared montmorillonite as bifunctional catalyst in eco-friendly citronellal conversion. Eng J 19:43–53. https://doi.org/10.4186/ej.2015.19.5.43
7. da Silva Rocha KA, Robles-Dutenhefner PA, Sousa EMB et al (2007) Pd-heteropoly acid as a bifunctional heterogeneous catalyst for one-pot conversion of citronellal to menthol. Appl Catal A 317:171–174. https://doi.org/10.1016/j.apcata.2006.10.019
8. Milone C, Gangemi C, Neri G et al (2000) Selective one step synthesis of (-)menthol from (+)citronellal on Ru supported on modified SiO_2. Appl Catal A 199:239–244. https://doi.org/10.1016/S0926-860X(99)00560-8
9. Azkaar M, Mäki-Arvela P, Vajglová Z et al (2019) Synthesis of menthol from citronellal over supported Ru- and Pt-catalysts in continuous flow. React Chem Eng 4:2156–2169. https://doi.org/10.1039/c9re00346k
10. Vajglová Z, Kumar N, Peurla M et al (2020) Cascade transformations of (±)-citronellal to menthol over extruded Ru-MCM-41 catalysts in a continuous reactor. Catal Sci Technol 10:8108–8119. https://doi.org/10.1039/d0cy01251c
11. Trasarti AF, Marchi AJ, Apesteguía CR (2004) Highly selective synthesis of menthols from citral in a one-step process. J Catal 224:484–488. https://doi.org/10.1016/j.jcat.2004.03.016
12. Mäki-Arvela P, Kumar N, Nieminen V et al (2004) Cyclization of citronellal over zeolites and mesoporous materials for production of isopulegol. J Catal 225:155–169. https://doi.org/10.1016/j.jcat.2004.03.043
13. Ten Dam J, Ramanathan A, Djanashvili K et al (2017) Synthesis, characterization and performance of bifunctional catalysts for the synthesis of menthol from citronellal. RSC Adv 7:12041–12053. https://doi.org/10.1039/c6ra25931f
14. Cortés CB, Galván VT, Pedro SS, García TV (2011) One pot synthesis of menthol from (±)-citronellal on nickel sulfated zirconia catalysts. Catal Today 172:21–26. https://doi.org/10.1016/j.cattod.2011.05.005
15. Plößer J, Lucas M, Claus P (2014) Highly selective menthol synthesis by one-pot transformation of citronellal using Ru/H-BEA catalysts. J Catal 320:189–197. https://doi.org/10.1016/j.jcat.2014.10.007
16. Adilina IB, Pertiwi R, Sulaswatty A (2015) Conversion of (±) -citronellal and its derivatives to (—) -menthol using bifunctional nickel zeolite catalysts. Biopropal Industri 6:1–6
17. Chauvel A, Delmon B, Hölderich WF (1994) New catalytic processes developed in Europe during the 1980's. Appl Catal A 115:173–217. https://doi.org/10.1016/0926-860X(94)80353-6
18. Jäkel C, Paciello R (2009) Method for the production of optically active carbonyl, United States US Patent 7.534,921 B2.
19. Vandichel M, Vermoortele F, Cottenie S et al (2013) Insight in the activity and diastereoselectivity of various lewis acid catalysts for the citronellal cyclization. J Catal 305:118–129. https://doi.org/10.1016/j.jcat.2013.04.017
20. Jimeno C, Miras J, Esquena J (2014) Hafnia–silica cryogels: solvent-assisted textural and catalytic control in the citronellal cyclization. ChemCatChem 6:2626–2633. https://doi.org/10.1002/CCTC.201402189
21. Iftitah ED, Muchalal M, Trisunaryanti W et al (2011) One pot transformation of citronellal to menthol over Ni/γ-Al_2O_3. J Appl Sci Res 7:680–689
22. Yadav GD, Nair JJ (1998) Novelties of eclectically engineered sulfated zirconia and carbon molecular sieve catalysts in cyclisation of citronellal to isopulegol. Chem Commun. https://doi.org/10.1039/a806815a
23. Nie Y, Chuah GK, Jaenicke S (2006) Domino-cyclisation and hydrogenation of citronellal to menthol over bifunctional Ni/Zr-Beta and Zr-beta/Ni-MCM-41 catalysts. Chem Commun. https://doi.org/10.1039/b513430g
24. Nie Y, Niah W, Jaenicke S, Chuah GK (2007) A tandem cyclization and hydrogenation of (±)-citronellal to menthol over bifunctional Ni/Zr-beta and mixed Zr-beta and Ni/MCM-41. J Catal 248:1–10. https://doi.org/10.1016/j.jcat.2007.02.018
25. Trasarti AF, Marchi AJ, Apesteguía CR (2007) Design of catalyst systems for the one-pot synthesis of menthols from citral. J Catal 247:155–165. https://doi.org/10.1016/j.jcat.2007.01.016
26. Mihailova B, Valtchev V, Mintova S et al (2005) Interlayer stacking disorder in zeolite beta family: a Raman spectroscopic study. Phys Chem Chem Phys 7:2756–2763. https://doi.org/10.1039/b503150h
27. Mintova S, Reinelt M, Senker J et al (2003) Pure silica BETA colloidal zeolite assembled in thin films. Chem Commun 3:326–327. https://doi.org/10.1039/b210767h
28. Kuehl GH, Timken HKC (2000) Acid sites in zeolite Beta: Effects of ammonium exchange and steaming. Microporous Mesoporous Mater 35:521–532. https://doi.org/10.1016/S1387-1811(99)00247-4
29. Balu AM, Campelo JM, Luque R, Romero AA (2010) One-step microwave-assisted asymmetric cyclisation/hydrogenation of citronellal to menthols using supported nanoparticles on mesoporous materials. Org Biomol Chem 8:2845–2849. https://doi.org/10.1039/c003600e
30. Mertens P, Verpoort F, Parvulescu AN, de Vos D (2006) Pt/H-beta zeolites as productive bifunctional catalysts for the one-step citronellal-to-menthol conversion. J Catal 243:7–13. https://doi.org/10.1016/j.jcat.2006.06.017
31. Nie Y, Jaenicke S, Chuah GK (2009) Zr–Zeolite beta a new heterogeneous catalyst system for the highly selective cascade transformation of citral to (+)-menthol. Chem—A Eur J 15:1991–1999. https://doi.org/10.1002/CHEM.200801776
32. Lutterotti L (2010) Total pattern fitting for the combined size-strain-stress-texture determination in thin film diffraction. Nucl Instrum Methods Phys Res, Sect B 268:334–340. https://doi.org/10.1016/j.nimb.2009.09.053

33. Emeis CA (1993) Determination of integrated molar extinction coefficients for infrared absorption bands of pyridine adsorbed on solid acid catalysts. J Catal. https://doi.org/10.1006/jcat.1993.1145
34. Lanzafame P, Perathoner S, Centi G et al (2017) Effect of the structure and mesoporosity in Ni/zeolite catalysts for n-hexadecane hydroisomerisation and hydrocracking. ChemCatChem 9:1632–1640. https://doi.org/10.1002/cctc.201601670
35. Martínez-Franco R, Paris C, Martínez-Armero ME et al (2016) High-silica nanocrystalline Beta zeolites: efficient synthesis and catalytic application. Chem Sci 7:102–108. https://doi.org/10.1039/c5sc03019f
36. Wei X, Li Y, Hua Z et al (2020) One-pot synthesized nickel-doped hierarchically porous Beta zeolite for enhanced methanol electrocatalytic oxidation activity. ChemCatChem 12:6285–6290. https://doi.org/10.1002/cctc.202001363
37. Wang S, He B, Tian R et al (2018) Ni-hierarchical Beta zeolite catalysts were applied to ethanol steam reforming: effect of sol gel method on loading Ni and the role of hierarchical structure. Mol Catal 453:64–73. https://doi.org/10.1016/j.mcat.2018.04.034
38. Vajglová Z, Kumar N, Peurla M et al (2018) Synthesis and physicochemical characterization of beta zeolite-bentonite composite materials for shaped catalysts. Catal Sci Technol 8:6150–6162. https://doi.org/10.1039/c8cy01951g
39. Cañizares P, de Lucas A, Dorado F et al (1998) Characterization of Ni and Pd supported on H-mordenite catalysts: influence of the metal loading method. Appl Catal A 169:137–150. https://doi.org/10.1016/S0926-860X(98)00008-8
40. Popova M, Djinović P, Ristić A et al (2018) Vapor-phase hydrogenation of levulinic acid to γ-valerolactone over bi-functional Ni/HZSM-5 catalyst. Front Chem 6:1–12. https://doi.org/10.3389/fchem.2018.00285
41. Peron DV, Zholobenko VL, de la Rocha MR, Oberson de Souza M, Feris LA, Marcilio NR, Ordomsky VV, Khodakov AY (2019) Nickel–zeolite composite catalysts with metal nanoparticles selectively encapsulated in the zeolite micropores. J Mater Sci 54:5399–5411. https://doi.org/10.1007/s10853-018-03250-5
42. Karthikeyan D, Lingappan N, Sivasankar B (2008) Effect of Ni in palladium β-zeolite on hydroisomerization of n-decane. Korean J Chem Eng 25:987–997. https://doi.org/10.1007/s11814-008-0160-9
43. Yoshioka CMN, Garetto T, Cardoso D (2005) N-hexane isomerization on Ni-Pt catalysts/supported on HUSY zeolite: the influence from a metal content. Catal Today 107–108:693–698. https://doi.org/10.1016/j.cattod.2005.07.056
44. Losch P, Huang W, Vozniuk O et al (2019) Modular Pd/zeolite composites demonstrating the key role of support hydrophobic/hydrophilic character in methane catalytic combustion. ACS Catal 9:4742–4753. https://doi.org/10.1021/acscatal.9b00596
45. Ji X, Qin Z, Dong M et al (2007) Friedel-Crafts acylation of anisole and toluene with acetic anhydride over nano-sized Beta zeolites. Catal Lett 117:171–176. https://doi.org/10.1007/s10562-007-9131-8
46. Li J, Liu H, An T et al (2017) Carboxylic acids to butyl esters over dealuminated-realuminated beta zeolites for removing organic acids from bio-oils. RSC Adv 7:33714–33725. https://doi.org/10.1039/c7ra05298g
47. Tieuli S, Mäki-Arvela P, Peurla M et al (2019) Hydrodeoxygenation of isoeugenol over Ni-SBA-15: kinetics and modelling. Appl Catal A 580:1–10. https://doi.org/10.1016/j.apcata.2019.04.028
48. Niculescu M, Budrugeac P (2013) Structural characterization of nickel oxide obtained by thermal decomposition of polynuclear coordination compound [Ni2(OH) 2(H3CCH(OH)COO-)2(H2O)2·0.5H2O]n. Rev Roum Chim 58:381–386
49. Richardson JT, Scates R, Twigg MV (2003) X-ray diffraction study of nickel oxide reduction by hydrogen. Appl Catal A 246:137–150. https://doi.org/10.1016/S0926-860X(02)00669-5
50. Torozova A, Mäki-Arvela P, Aho A et al (2015) Heterogeneous catalysis for transformation of biomass derived compounds beyond fuels: synthesis of monoterpenoid dioxinols with analgesic activity. J Mol Catal A: Chem 397:48–55. https://doi.org/10.1016/j.molcata.2014.10.023
51. Bermejo-López A, Pereda-Ayo B, González-Marcos JA, González-Velasco JR (2019) Ni loading effects on dual function materials for capture and in-situ conversion of CO_2 to CH_4 using CaO or Na_2CO_3. J CO2 Util 34:576–587. https://doi.org/10.1016/j.jcou.2019.08.011
52. Yang Y, Ghildiyal P, Zachariah MR (2019) Thermal shock synthesis of metal nanoclusters within on-the-fly graphene particles. Langmuir 35:3413–3420. https://doi.org/10.1021/acs.langmuir.8b03532
53. Fetohi AE, Amin RS, Hameed RMA, El-Khatib KM (2017) Effect of nickel loading in Ni@Pt/C electrocatalysts on their activity for ethanol oxidation in alkaline medium. Electrochim Acta 242:187–201. https://doi.org/10.1016/j.electacta.2017.05.022
54. Bergeret G, Gallezot P (2008) Particle size and dispersion measurements. In: Ertl G, Weitkamp J (eds) Handbook of Heretogeneous Catalysis. Wiley, Weinheim
55. Kubička D, Kumar N, Venäläinen T et al (2006) Metal-support interactions in zeolite-supported noble metals: influence of metal crystallites on the support acidity. J Phys Chem B 110:4937–4946. https://doi.org/10.1021/jp055754k
56. Taghavi S, Ghedini E, Menegazzo F et al (2022) CuZSM-5@HMS composite as an efficient micro-mesoporous catalyst for conversion of sugars into levulinic acid. Catal Today 390–391:146–161. https://doi.org/10.1016/j.cattod.2021.11.038
57. Venkatesha NJ, Bhat YS, Jai Prakash BS (2016) Dealuminated BEA zeolite for selective synthesis of five-membered cyclic acetal from glycerol under ambient conditions. RSC Adv 6:18824–18833. https://doi.org/10.1039/c6ra01437b
58. Crémoux T, Batonneau-Gener I, Moissette A et al (2019) Influence of framework Si/Al ratio and topology on electron transfers in zeolites. Phys Chem Chem Phys 21:14892–14903. https://doi.org/10.1039/c9cp01166h
59. Vajglová Z, Simakova IL, Eränen K et al (2022) The physicochemical and catalytic properties of clay extrudates in cyclization of citronellal. Appl Catal A 629:1–11. https://doi.org/10.1016/j.apcata.2021.118426
60. Chuah GK, Liu SH, Jaenicke S, Harrison LJ (2001) Cyclisation of citronellal to isopulegol catalysed by hydrous zirconia and other solid acids. J Catal 200:352–359. https://doi.org/10.1006/jcat.2001.3208
61. Zhivonitko VV, Vajglová Z, Mäki-Arvela P et al (2021) Diffusion measurements of hydrocarbons in zeolites with pulse-field gradient nuclear magnetic resonance spectroscopy. Russ J Phys Chem A 95:547–557. https://doi.org/10.1134/S0036024421030250
62. Vajglová Z, Kumar N, Mäki-Arvela P et al (2019) Synthesis and physicochemical characterization of shaped catalysts of β and Y zeolites for cyclization of citronellal. Ind Eng Chem Res 58:18084–18096. https://doi.org/10.1021/acs.iecr.9b02829
63. Shah AK, Maitlo G, Shah AA et al (2019) One pot menthol synthesis via hydrogenations of citral and citronellal over montmorillonite-supported Pd/Ni-heteropoly acid bifunctional catalysts. React Kinet Mech Catal 128:917–934. https://doi.org/10.1007/s11144-019-01679-6

64. Pertiwi R, Tursiloadi S, Adilina IB et al (2017) Nickel supported natural zeolite as a bifunctional catalysts for conversion of citronella oil crude to menthols. J Kim Terap Indonesia 18:132–138. https://doi.org/10.14203/jkti.v18i02.78

Authors and Affiliations

Somayeh Taghavi[1,2] · Päivi Mäki-Arvela[1] · Zuzana Vajglová[1] · Markus Peurla[3] · Ilari Angervo[4] · Kari Eränen[1] · Elena Ghedini[2] · Federica Menegazzo[2] · Mojgan Zendehdel[5] · Michela Signoretto[2] · Dmitry Yu. Murzin[1]

✉ Michela Signoretto
miky@unive.it

✉ Dmitry Yu. Murzin
dmurzin@abo.fi

[1] Johan Gadolin Process Chemistry Centre, Åbo Akademi University, Henriksgatan 2, 20500 Turku/Åbo, Finland

[2] CATMAT Lab, Department of Molecular Sciences and Nanosystems, Ca' Foscari University of Venice and INSTM RUVe, via Torino 155, 30172 Venezia Mestre, Italy

[3] Institute of Biomedicine, University of Turku, Kiinamyllynkatu 10, 20520 Turku, Finland

[4] Wihuri Physical Laboratory, Department of Physics and Astronomy, University of Turku, 20014 Turku, Finland

[5] Chemistry Department, Faculty of Sciences, Arak University, Dr. Beheshti Ave, Arak 38156-88349, Iran